Alberta Thy 8-15, Fermilab-PUB-15-205-PPD

High-energy electrons from the muon decay in orbit: radiative corrections

Robert Szafron and Andrzej Czarnecki
Department of Physics, University of Alberta, Edmonton, Alberta, Canada T6G 2G7

We determine the $\mathcal{O}(\alpha)$ correction to the energy spectrum of electrons produced in the decay of muons bound in atoms. We focus on the high-energy end of the spectrum that constitutes a background for the muon-electron conversion and will be precisely measured by the upcoming experiments Mu2e and COMET. The correction suppresses the background by about 20%.

PACS numbers: 13.35.Bv, 36.10.Ee

In matter, muons decay differently from antimuons. Although the decay rates are very similar [1], negatively charged μ^- can bind with nuclei. The nucleus exchanges photons with the muon and the daughter electron, rearranging the energy distribution. In this paper we find how this rearrangement is affected by the real radiation and self-interaction on the muon-electron line. We predict the energy spectrum of the highest-energy electrons, interesting both theoretically and experimentally.

From the theoretical standpoint, the muon decay is the simplest example with which to study the dynamics of an unstable particle and to develop a theory of the various binding effects, including the motion in the initial state, interplay of the binding and the self-interaction, and the recoil of the nucleus. On the experimental side, the bound muon decay has recently been measured [2] with a precision sufficient to probe radiative corrections, subsequently evaluated in [3]; however, those measurements focused on the lower half of the spectrum that is also accessible to a free muon decay.

Interestingly, the energy range of electrons produced in a decay of a muon bound in an atom (decay in orbit, DIO) reaches to about twice the maximum possible in a free-muon decay. When the muon decays in vacuum, momentum conservation requires that at least half of the energy be carried away by the neutrinos. In the DIO, the nucleus can absorb the momentum without taking much energy, because it is so much heavier than the muon.

The high-energy part is important for the upcoming experiments COMET in J-PARC [4] and Mu2e in Fermilab [5]. Searching for the ultra-rare neutrinoless muon-electron conversion, these studies will collect a large sample of events with high-energy electrons. Their designs foresee a sensitivity better than one exotic conversion for 10^{16} ordinary muon decays. The signature of the exotic process is a monochromatic electron excess at the maximum energy. These experiments need a reliable prediction of the high-energy spectrum to distinguish an exotic signal from the Standard Model background.

Predicting the DIO spectrum is a challenge because both the decaying muon and the daughter electron interact with the Coulomb field of the nucleus. A numerical calculation with Coulomb-Dirac wave functions is possible [6] provided that self-interactions (photons attached to the muon and the electron) are neglected. How can they be included? In the lower half of the spectrum the muon and the electron can be treated as nearly free and the bound state effects can be factorized. Then the radiative corrections calculated for a free muon are convoluted with a shape function that parametrizes the Coulomb field effect [3, 7]. In the present paper we construct for the first time an expansion around the end-point, that allows us to systematically include radiative corrections to the high-energy part of the spectrum.

Accounting for the external Coulomb field in charged-particle propagators is called the Furry picture [8]. In this formulation, and still ignoring radiative corrections, a single diagram, shown in Fig. 1, describes the DIO. We shall demonstrate that the bound-state radiative

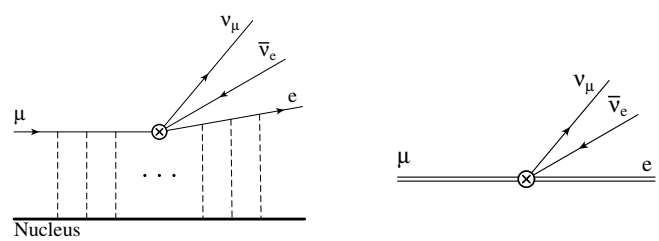

FIG. 1. Muon decay in orbit (DIO). The left panel shows the exchange of Coulomb photons (dashed lines) between charged leptons and the nucleus. The right pannel represents the same physics using double lines for charged fermions propagating in the external Coulomb field (Furry picture).

corrections are easiest to evaluate near the high-energy end of the spectrum, that is the most important part for the new experiments. For now we neglect the nuclear recoil and structure, and treat the nucleus as an infinitely-heavy point source of a Coulomb field. We denote the electron energy with E; its maximum value is $E_{\max} = m_\mu \left(1 - \frac{(Z\alpha)^2}{2}\right)$, where m_μ is muon mass, Z is the atomic number, and $\alpha \simeq 1/137$ is the fine-structure constant. The DIO spectrum can be expanded near its end-point in the small parameter $\Delta = \frac{E_{\max}-E}{m_\mu}$,

$$\frac{m_\mu}{\Gamma_0}\frac{\mathrm{d}\Gamma}{\mathrm{d}E} = \sum_{ijk} B_{ijk}\Delta^i(\pi Z\alpha)^j\left(\frac{\alpha}{\pi}\right)^k. \qquad (1)$$

Operated by Fermi Research Alliance, LLC under Contract No. De-AC02-07CH11359 with the United States Department of Energy.

Powers of $\pi Z\alpha$ parameterize photon exchanges with the nucleus and α/π arises from radiative corrections on the charged-lepton line and the vacuum polarization. The first non-vanishing term has $i = j = 5$ and $k = 0$, with $B_{550} = \frac{1024}{5\pi^6} \simeq 0.21$. In higher-order terms, coefficients B may contain logarithms of $Z\alpha$ and Δ, as we shall see.

Corrections to this leading behavior have several sources, among which higher-order binding effects are the most important. There are some theoretical similarities between the DIO and the photoelectric effect that we shall exploit. Binding effects in both are described as an expansion in $\pi Z\alpha$ [9, 10] rather than $Z\alpha$. Indeed, a numerical evaluation for a point-like nucleus with $Z = 13$ (corresponding to aluminum, the planned target in COMET and Mu2e) finds a -21% correction, consistent with $13\pi\alpha = 0.3$. Logarithmic enhancement begins with $(\pi Z\alpha)^7 \ln(Z\alpha)$. Fortunately, these large effects are summed up in the numerical evaluation [6].

The next source of corrections is the finite nuclear size, also included in [6]. We will comment at the end of this paper on how to refine them. The largest of all the corrections, they slightly suppress higher orders in $Z\alpha$. The finite nuclear mass introduces a recoil effect, also evaluated in [6]. It has only a small effect on the coefficients B but it shifts the end-point energy $E_{\max}$.

Finally, the most challenging corrections result from radiative effects that are the subject of this study. Before we discuss technical details, we present our main result. Close to the end-point, including radiative corrections, the DIO spectrum for aluminum can be written as

$$\frac{m_\mu}{\Gamma_0}\frac{\mathrm{d}\Gamma}{\mathrm{d}E} \approx \left(1.44\,\Delta^{0.023} - 0.22\right) \times 10^{-4}\,\Delta^5. \qquad (2)$$

To illustrate the importance of the new corrections we consider the last 150 keV of the spectrum (this is the typical planned resolution of Mu2e and COMET). Radiative corrections reduce the number of events in this bin by 19%, a welcome reduction of the background.

In the remainder we explain the origin of such a large effect. First we want to clarify how electrons can acquire the energy of the full muon mass, even though a free muon decay produces electrons with at most half that energy. A large amount of three-momentum must be transferred to the nucleus, instead of sharing the energy with neutrinos. We will argue that this happens predominantly via an exchange of a single, highly virtual photon, rather than through many interactions.

The relativistic electron is described by a plane wave distorted by the Coulomb potential V,

$$\overline{\psi}_p\left(\vec{q}\right) = \bar{u}(p)\left[\delta^3\left(\vec{p}-\vec{q}\right) + \not{V}\left(\left(\vec{p}-\vec{q}\right)^2\right)\frac{1}{\not{q}-m_e}\right], \qquad (3)$$

where $u(p)$ is a spinor solution of a free Dirac equation and the four-potential in momentum space reads

$$V\left(\vec{k}^2\right) = \left(-\frac{Z\alpha}{2\pi^2\vec{k}^2}, \vec{0}\right). \qquad (4)$$

A muon bound to a nucleus with $Z \ll 137$ is nonrelativistic. Nevertheless, we will need the first relativistic correction to its wave function, just like in the classic analysis of the photoelectric effect [11],

$$\psi\left(\vec{q}\right) = \psi_{\mathrm{NR}}\left(\vec{q}\right)\left(1 + \frac{\vec{q}\cdot\vec{\gamma}}{2m_\mu}\right)u(P) \qquad (5)$$

where $\psi_{\mathrm{NR}}\left(\vec{q}\right) = \frac{8\pi Z\alpha m_\mu \Psi(0)}{[\vec{q}^2+(Z\alpha m_\mu)^2]^2}$ is the nonrelativistic momentum-space wave function of the 1S ground state with $\Psi(0) = \left(\frac{Z\alpha m_\mu}{\pi^{1/3}}\right)^{3/2}$; $u(P)$ is a four-spinor of a muon at rest, $P = (m_\mu, 0)$.

We now consider separately the contributions of the two terms in the electron wave function (3). The delta function term forces the muon momentum in (5) to be large, $\vec{q} = \vec{p} \sim m_\mu$. Thus we neglect $Z\alpha m_\mu$ in the denominator of ψ_{NR} and find

$$\psi\left(\vec{q}\right) \approx (2\pi)^3\Psi(0)\frac{1}{\not{P}+\not{q}-m}\not{V}\left(\vec{q}^2\right)u(P). \qquad (6)$$

This is visualized in Fig. 2a: the muon, before decaying, transfers momentum $\vec{q} \sim m_\mu$ to the nucleus through a hard space-like photon. It is here that the relativistic correction to the muon wave function is important.

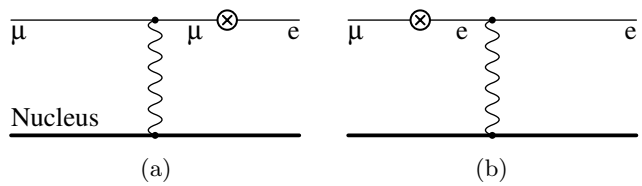

FIG. 2. Furry diagram expanded in $Z\alpha$. Crossed circles indicate insertions of the weak interaction transforming the muon into an electron; the emitted neutrinos are not shown. These two amplitudes give rise to the highest-energy electrons.

The second term in (3) refers to an electron scattered on the nucleus. There is no δ-function restricting the μ momentum to large values; the muon introduces into the matrix element its typical bound-state momentum $\vec{q} \sim Z\alpha m_\mu$, negligible in comparison with $\vec{p} \sim m_\mu$. We use $\lim_{a\to 0}\frac{8\pi a}{(q^2+a^2)^2} = (2\pi)^3\delta^3\left(\vec{q}\right)$ to approximate the muon wave function by

$$\psi\left(\vec{q}\right) \approx (2\pi)^3\Psi(0)\delta^3\left(\vec{q}\right)u(P). \qquad (7)$$

This is shown in Fig. 2b, where the hard photon is exchanged after the decay.

An evaluation of both diagrams in Fig. 2 gives the leading contribution B_{550} in (1). We note that in both cases no energy is transfered to the nucleus and any energy unused by the electron ($\sim \Delta$) is taken up by the neutrinos. Counting the powers of neutrino momenta in the integrated matrix element,

$$\int \frac{\mathrm{d}^3\nu}{\nu_0}\frac{\mathrm{d}^3\overline{\nu}_0}{\overline{\nu}_0}\delta\left(m_\mu\Delta - \nu_0 - \overline{\nu}_0\right)\ldots\psi\ldots\overline{\psi} \sim \Delta^5, \qquad (8)$$

explains the leading energy dependence in (1).

Having understood that only two diagrams describe the end-point behavior, we are now ready to evaluate radiative corrections. In the Furry picture there are two groups of virtual corrections, shown in Fig. 3. We expand them in $Z\alpha$ just like the tree-level diagrams, except that in addition to the expansion of wave functions (3, 5), we

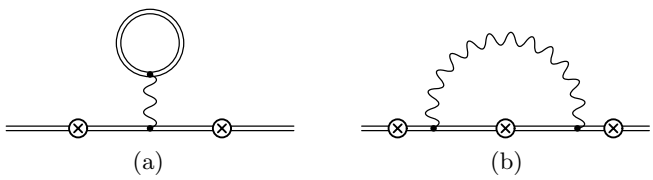

FIG. 3. Virtual corrections to the muon DIO in the Furry picture.

also need the Coulomb-Dirac Green's function [12],

$$-iG^V(E;\vec{p},\vec{p}') \simeq \frac{\delta^3\left(\vec{p}-\vec{p}'\right)}{\not{p}-m} + \frac{1}{\not{p}-m}\not{V}\left((\vec{p}-\vec{p}')^2\right)\frac{1}{\not{p}'-m}. \quad (9)$$

Due to the external field, the Green's function depends separately on $\vec{p}$ and $\vec{p}'$ and not only on $\vec{p}$. Expansion (9) generates loop diagrams that we evaluate analytically using standard techniques [13].

For example, the leading approximation of the diagram 3a gives a one-loop vacum polarization insertion into the photon propagators in Fig. 2. It enhances the tree-level decay rate by a factor $1+\frac{\alpha}{\pi}\delta_{\rm VP}$, with

$$\delta_{\rm VP} = \frac{4}{3}\ln\frac{m_\mu}{m_e} - \frac{10}{9} + 0.12 \approx 6.1, \quad (10)$$

where the term 0.12 arises from a muon loop. The enhancement of about 1.4% reflects the running of the electromagnetic coupling, significant when either the muon or the daughter electron are close to the nucleus.

Another correction comes from the real radiation. The set of diagrams represented by Fig. 4 is expanded in the

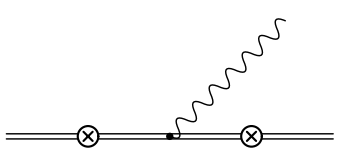

FIG. 4. Furry diagram for the real radiation correction.

same way as virtual corrections, using (9). Near the end-point it is sufficient to use the eikonal approximation since the energy conservation requires that the real photons be soft, $0 < E_\gamma < m_\mu\Delta$.

Virtual and real radiation, separately divergent, together give a finite correction,

$$\frac{B_{551}}{B_{550}} = -\frac{46}{15}\ln\frac{m_\mu}{m_e} + \delta_{\rm S}\ln\Delta + 0.76 + \delta_{\rm VP}, \quad (11)$$

with

$$\delta_{\rm S} = 2\ln 2 - 2 + 2\ln\frac{m_\mu}{m_e}. \quad (12)$$

The part enhanced by $\ln\frac{m_\mu}{m_e} = 5.33$, due to collinear photons, can be predicted using the electron structure function, providing a useful check. This is possible since the electron in the final state is relativistic, $E \gg m_e$, and corrections from the Coulomb potential to the electron structure function can be neglected.

Contributions of soft photons $\delta_{\rm S}$ can be exponentiated [14]. To separate the hard corrections, we introduce

$$\delta_{\rm H} = \frac{B_{551}}{B_{550}} - \delta_{\rm S}\ln\Delta \approx -9.5. \quad (13)$$

Then, denoting with a tilde a sum of only soft-photon contribution for $i > 1$, we find

$$\widetilde{\sum}_{i=0}^{\infty} B_{55i}\left(\frac{\alpha}{\pi}\right)^i = B_{550}\left[\Delta^{\frac{\alpha}{\pi}\delta_{\rm S}} + \frac{\alpha}{\pi}\delta_H\right]. \quad (14)$$

Now when $\Delta \to 0$, instead of unphysically diverging with $\ln\Delta$, the soft-photon correction vanishes.

So far we have assumed a point nucleus. The end-point is characterized by a large momentum transfer so the difference between a point and a finite nucleus matters. Fortunately, in the order in $\pi Z\alpha$ we are interested in, the bulk of this effect is an overall multiplicative factor.

From now on, we specialize to the case of aluminum, although the discussion can easily be applied to other nuclei. With that in mind, we keep the Z dependence explicit. We assume a Fermi charge distribution,

$$\varrho = \frac{\rho_0}{1+\exp\frac{r-r_0}{a_0}} \quad (15)$$

with $a_0 = 0.569$ fm and $r_0 = 2.84(5)$ fm [15].

Two factors should be corrected to include the finite size: the nucleus form-factor and the muon wave function at the origin. We define the form-factor as a ratio of Fourier transforms of potentials calculated for the extended charge distribution (15) and the point-like (4),

$$F_\rho(\vec{k}^2) = \frac{V_\rho\left(\vec{k}^2\right)}{V\left(\vec{k}^2\right)} \longrightarrow 0.64 \ \text{ for } \ \vec{k}^2 = m_\mu^2. \quad (16)$$

The muon wave function $\chi(x)$ is found numerically from the Schrödinger equation with the potential V_ρ. We define the ratio R of wave functions at the origin,

$$R = \frac{\chi(0)^2}{\Psi(0)^2} = 0.71. \quad (17)$$

Then the terms B^{ρ}_{55k} for a finite nucleus are obtained from respective terms for a point nucleus, in particular

$$B^{\rho}_{550} = RF^2_{\rho}(m^2_{\mu})B_{550} = 0.061. \tag{18}$$

The suppression due to the form-factor decreases also the higher-order binding effects.

Finally we estimate the recoil and the higher-order binding effects. Ref. [6] found the end-point behaviour for aluminum. We rewrite that result separating the leading from the higher-order (H.O.) effects,

$$B^{\rho}_{550}(\pi Z\alpha)^5 + \sum_{j=6}^{\infty} B^{\rho}_{5j0}\,(\pi Z\alpha)^j \equiv B^{\rho}_{550}(\pi Z\alpha)^5 + \text{H.O.}$$
$$= 8.98\times 10^{-17}\left(\frac{m_{\mu}}{\text{MeV}}\right)^6. \tag{19}$$

Now we include our radiative correction (14) in the leading order and get at order Δ^5

$$\frac{m_{\mu}}{\Gamma_0}\frac{\mathrm{d}\Gamma}{\mathrm{d}E} \approx \left[B^{\rho}_{550}\left(\Delta^{\frac{\alpha}{\pi}\delta_{\text{S}}} + \frac{\alpha}{\pi}\delta_{\text{H}}\right)(\pi Z\alpha)^5 + \text{H.O.}\right]\Delta^5. \tag{20}$$

With H.O. $= -1.9\times 10^{-5}$ [from (18) and (19)], this leads to our final result (2).

The increased exponent of Δ, due to soft corrections, suppresses the number of DIO events in the end-point region. The relative decrease is inversely correlated with the energy resolution: the number of electrons in the end-point bin of 1 (0.1) MeV is reduced by 15% (20%).

There are three main uncertainties in our result. The first is an uncertainty in B^{ρ}_{550} due to the finite nucleus size. The wave functions (5–7) refer to the Coulomb potential. Comparing with numerical solutions of the wave equation, we estimate the error in eq. (18) at about 12%. This affects the extraction of the H.O. terms and induces an error of 1.8 – 2.4% in the total coefficient of Δ^5, for bin sizes in the range 0.1 – 1 MeV.

The second uncertainty are the uncalculated hard corrections $\mathcal{O}\left((\alpha/\pi)^2\right)$. They are expected to be small, since at order $\frac{\alpha}{\pi}$ the hard correction (13) is only 2.5%.

Further improvements of the DIO end-point prediction require a calculation of radiative corrections to the H.O. Assuming that they have the same relative effect as on B_{550}, we estimate the remaining uncertainty to be about 4% of the Δ^5 coefficient.

Even though the radiative corrections turn out to be large, knowing them we can assess the theoretical precision. We conservatively estimate the uncertainty of the number of events in the end-point bin to be about 6%.

To summarize, we have determined the correction to the high-energy tail of the DIO energy distribution and its remaining uncertainty. Key to this improvement has been the simplicity of the leading amplitudes that turn out to arise from a small number of hard-photon exchanges. This line of reasoning can be extended to higher-order binding effects, at least for a point nucleus. For a realistic charge distribution, a numerical evaluation of loop diagrams will be necessary. However, the leading radiative correction has now been established with good precision. Its sizeable negative effect on the DIO will make any observed event near the end-point an even more convincing signal of New Physics, a discovery we eagerly anticipate.

This research was supported by Natural Sciences and Engineering Research Council (NSERC) of Canada. R.S. acknowledges support by the Polish National Science Centre (NCN) under Grant Agreement No. DEC-2013/11/B/ST2/04023 and by the Fermilab Intensity Frontier Fellowship. Fermilab is operated by Fermi Research Alliance, LLC under Contract No. De-AC02-07CH11359 with the United States Department of Energy.

[1] A. Czarnecki, G. P. Lepage, and W. J. Marciano, Phys. Rev. **D61**, 73001 (2000).
[2] A. Grossheim *et al.* (TWIST Collaboration), Phys. Rev. **D80**, 052012 (2009).
[3] A. Czarnecki, M. Dowling, X. Garcia i Tormo, W. J. Marciano, and R. Szafron, Phys. Rev. **D90**, 093002 (2014), arXiv:1406.3575 [hep-ph].
[4] Y. Kuno (COMET Collaboration), PTEP **2013**, 022C01 (2013).
[5] D. Brown (Mu2e Collaboration), AIP Conf. Proc. **1441**, 596 (2012).
[6] A. Czarnecki, X. Garcia i Tormo, and W. J. Marciano, Phys. Rev. **D84**, 013006 (2011), arXiv:1106.4756 [hep-ph].
[7] R. Szafron and A. Czarnecki, "Shape function in QED and bound muon decays," Alberta Thy 9-15.
[8] W. Furry, Phys. Rev. **81**, 115 (1951).
[9] R. Pratt, A. Ron, and H. Tseng, Rev. Mod. Phys. **45**, 273 (1973).
[10] J. Eichler and T. Stöhlker, Phys. Rep. **439**, 1 (2007).
[11] V. B. Berestetsky, E. M. Lifshitz, and L. P. Pitaevsky, *Quantum Electrodynamics* (Pergamon, Oxford, 1982).
[12] J. Schwinger, *Particles, sources and fields*, Vol. 2 (Addison-Wesley, Redwood City, CA, 1973).
[13] A. V. Smirnov, Comput. Phys. Commun. **189**, 182 (2014), arXiv:1408.2372 [hep-ph].
[14] D. R. Yennie, S. C. Frautschi, and H. Suura, Ann. Phys. **13**, 379 (1961).
[15] H. de Vries *et al.*, At. Data and Nucl. Data Tables **36**, 495 (1987).